GEOPHYSICAL RESEARCH LETTERS, VOL. 19, NO. 20, PAGES 2071-2074, OCTOBER 23, 1992

IONOSPHERIC MODIFICATION WITH A VLF TRANSMITTER

U. S. Inan, J. V. Rodriguez, S. Lev-Tov, and J. Oh

Space, Telecommunications and Radioscience Laboratory, Stanford University, California

Abstract. Detectable heating of the nighttime D region by a 28.5 kHz signal is observed in 16 out of 144 cases with events occurring under conditions of moderate to low D region electron densities as represented by the unperturbed VLF signal levels. Three dimensional modeling of the effects of NAU heating on a probe VLF signal predicts values in general agreement with observations and suggests that maximum effects should occur under tenuous D region conditions.

1. Introduction

The first experimental evidence of heating of the nighttime lower ionosphere by VLF radiation [*Inan*, 1990], as predicted earlier by *Galejs* [1972], has raised new questions concerning ionospheric heating by VLF versus HF waves [*Dowden and Adams*, 1991; *Taranenko et al.*, 1992] and has led to the realization that VLF energy from lightning discharges can significantly modify the ionosphere [*Inan et al.*, 1991]. In this paper, we provide further experimental data on VLF transmitter heating and analyze results in the light of a three dimensional model of the heated region and the resultant perturbation of a subionospheric VLF probe signal.

2. Experimental Results

A controlled VLF wave-injection experiment was carried out in 1989 with the 28.5 kHz NAU transmitter in Aguadilla, Puerto Rico (100 kW radiated power) over two different 2-month periods (May-June and Oct-Nov 1989). NAU operated with a 3sON/2sOFF format for two 15-min periods starting at 0335 and 0735 UT on 102 separate occasions during May and June 1989 and on 42 during October and November 1989. Superposed epoch (of 180 5-s data segments) and spectral analyses (of 15-min data segments) were conducted on the various VLF transmitter signals received at Palmer (Figure 1). Cross-modulation on the 24.0 kHz signal from the NAA transmitter observed at Palmer (i.e., NAA-Palmer) was detected as a temporal signature of the 3sON/2sOFF modulation (on superposed data) and as a spectral peak at 0.2 Hz [*Inan*, 1990]. Two examples are shown in Figure 2, illustrating respectively an amplitude decrease ($\Delta A < 0$) and increase ($\Delta A > 0$) during the 3sON period. The results of analysis of all of the available data are:

1) No cross-modulation was found on any of the other signals observed at Palmer, including NSS-Palmer (Figure 1).
2) Spectral peaks at 0.2 Hz (Figure 2), at least 1 dB above any other frequency component >0.1 Hz, were found on the NAA-Palmer signal in 7 out of 102 keying episodes during May/June and 9 out of 42 episodes during Oct/Nov 1989, as summarized in Table 1. Both positive and negative amplitude changes (Figure 2) were observed, with absolute magnitudes ranging from 0.03 to 0.12 dB. The detection threshold is estimated to be ~0.01 dB.
3) Occurrence of events did not depend on geomagnetic activity (ΣKp) (Table 1). But 0.2 Hz peaks were observed under moderate lower ionospheric conditions, as represented by the unperturbed vertical component of the electric field (A) of the NAA signal at Palmer (Figure 3).
4) Spectral and superposed epoch analysis on the phase of the NAA-Palmer signal did not reveal any clear signatures of cross modulation, possibly due to interference from radio atmospherics causing the phase receiver to temporarily lose lock and leading to the presence of many large spikes (about 30 per min of $\geq 40°$). Detailed analysis of the phase data in our best cases indicates that the minimum detectable 3sON/2sOFF signature without superposition is 4°.

3. Structure of the Heated Region

Three ambient nighttime profiles are considered (Figure 4a); Profile I is an exponential [*Wait and Spies*, 1964] and Profile II represents typical conditions and was used in recent work [*Taranenko et al.*, 1992]. The three profiles crudely repre-

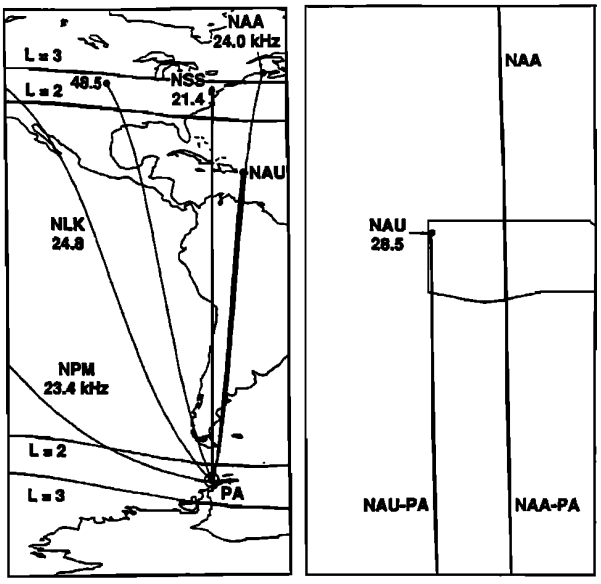

Fig. 1. Observation geometry of various VLF transmitter Great Circle Paths (GCP) to Palmer (PA) Station, Antarctica. The NAA-Palmer path crosses within ~57 km of the NAU transmitter (right hand panel). The loci of the feet of the $L = 2$ and $L = 3$ field lines at 100 km altitude are shown for reference. The NLK and the NPM transmitters are located respectively at (48°N,122°W) and (21°N,158°W). Associated with each transmitter is the operation frequency in kHz.

Paper number 92GL02378
0094-8534/92/92GL-02378$03.00

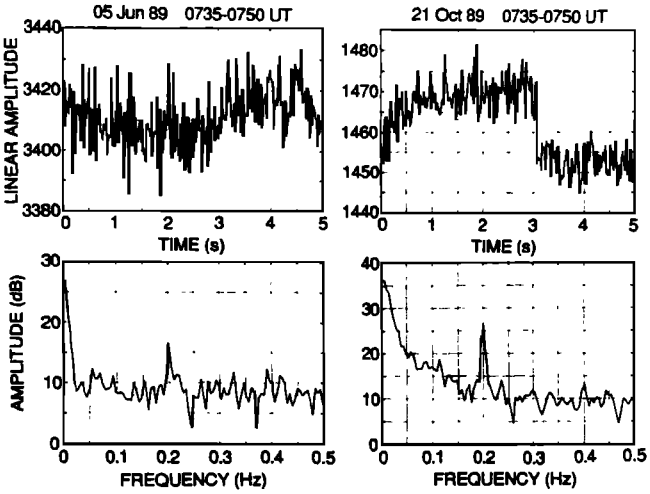

Fig. 2. The upper panels show the amplitude of the NAA signal at Palmer as a superposition of 180 5-s segments from the 0735-0750 UT periods on 5 Jun and 21 Oct 89. The vertical axis shows amplitude (A) in linear arbitrary units, with $A = 0$ being absence of signal. The lower panels show amplitude spectra of the 15-min data for the same periods.

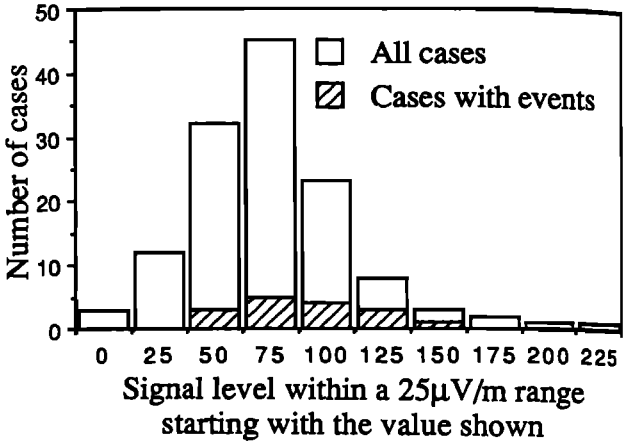

Fig. 3. Distribution of the number of observing periods as a function of the absolute intensity of the NAA-Palmer signal. Separately shown (cross-hatched) is the distribution of the number of periods with detectable events.

sent a 1:10:100 electron density ratio in the important altitude range of 75-90 km. The density above 97 km (Profile I), 90 km (Profile II), and 95 km (Profile III) is given by the International Reference Ionosphere (IRI) [*Rawer et al.*, 1978].

The structure of the disturbance is determined by calculating heating along rays originating at the NAU transmitter spaced in azimuth and elevation so as to illuminate points on a two-dimensional horizontal grid at a given altitude. We assume a simple electrically short vertical radiator with a toroidal pattern, although the coastal location of NAU may lead to some asymmetry due to differences between ground and seawater conductivities. We use general magneto-ionic theory for refractive index n and a WKB formulation to estimate the absorbed wave power $U(h)$ and the electron heating. For a Maxwellian electron distribution, the modified electron collision frequency is given by $\nu = (\nu_o/2) + [(\nu_o/2)^2 + 2\nu_o U/3GN_e k_B T_o]^{\frac{1}{2}}$ where G is the average fraction of electron energy transferred in one collision, N_e is the electron density, k_B is Boltzmann's constant, and $T_o(= 300°K)$, ν_o are the ambient electron temperature and collision frequency [*Maslin*, 1974]. Self absorption is accounted for by computing $\Delta\nu$ at ~0.1 km altitude steps and adding $\Delta\nu$ from the previous step to the ambient ν_o at the next step to determine the new ν (i.e., $\nu^h = \nu_o^h + \Delta\nu^{h-\Delta h}$) that is used to estimate n and thus the new $\Delta\nu$ (and ΔT since $\Delta T/T_o \simeq \Delta\nu/\nu_o$) [*Inan et al.*,1991]. The G is assumed $\sim 1.3\times10^{-3}$ to provide continuity with earlier work [*Maslin*, 1974; *Inan*, 1990], although it varies with T, depends on neutral composition and temperature, and can be 2-3 times higher [*Gurevich*, 1978, p.86]. For weak heating, $\Delta\nu$ is proportional to G^{-1}.

The normalized heated electron temperature, $T_n(h) = 1 + \Delta T/T_o$, is shown in Figure 4b for the three different ambient profiles (Figure 4a). The smaller peak at the higher altitude is due to the extraordinary wave [*Inan*, 1990]. The largest $\Delta\nu$ is expected for the most tenuous D region (Profile I).

The T_n for Profile II at 77.9 km altitude is plotted in Figure 5a over a 500 km × 500 km area centered above NAU. The central null is due to the antenna radiation pattern while the north-south asymmetry is due to the dependence of absorption on the angle between the wave vector and the Earth's magnetic

TABLE 1. Experimental Results.

Date	Time (UT)	ΔA (dB)	Peak (dB)	ΣKp	A (μV/m)
07May89	0335	+0.07	5	37	95
15May89	0335	+0.09	2	22	71
18May89	0735	+0.05	3	13	103
28May89	0735	+0.05	2	22	95
05Jun89	0735	-0.03	5	14	134
13Jun89	0335	+0.05	5	23	103
16Jun89	0335	+0.12	4	15	55
21Oct89	0335	+0.12	2	57	100
	0735	+0.10	7	57	175
24Oct89	0735	+0.04	2	25	150
25Oct89	0735	+0.07	1	25	138
29Oct89	0335	+0.10	5	21	88
30Oct89	0335	+0.11	4	29	88
05Nov89	0335	+0.03	2	27	125
	0735	-0.04	3	27	125
14Nov89	0735	+0.10	5	21	63

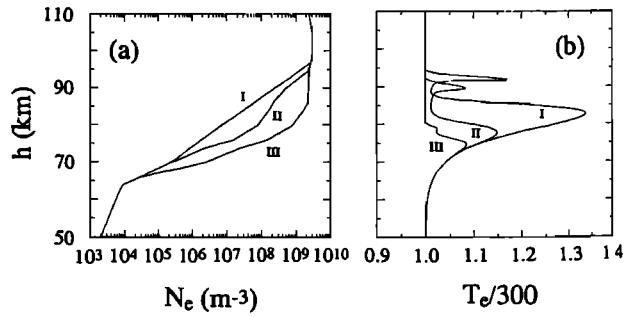

Fig. 4. (a) The three different nighttime ambient density models used in this paper. Profiles I and III represent the extremes of electron density in the critical altitude range of 70-90 km, with Profile II being the typical ambient used in other work [*Poulsen et al.*, 1992]. (b) The corresponding altitude profiles of electron temperature due to heating by the NAU transmitter signal above and below the point of peak heating.

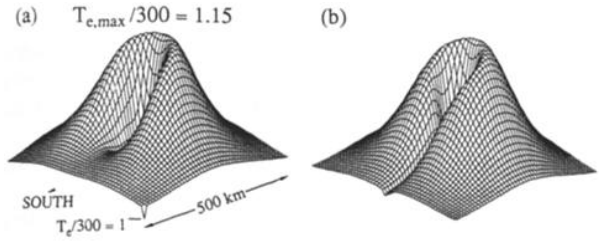

Fig. 5. (a) The transverse structure of the heated region (in terms of T_e normalized to 300° K) at 77.9 km (altitude of maximum heating) for the typical ambient case (Profile II). (b) Analytical approximation to (a).

field [*Galejs*, 1972]. The wave electric field is parallel to the static magnetic field and the absorption rate is maximized for rays emanating from NAU at 41° elevation and magnetic north azimuth. This anisotropy is important only for low power VLF heating, for which the wave frequency ω and the heated ν are less than the gyrofrequency ω_H.

The transverse structure of the heated region varies only slightly over the altitude range of ordinary-mode heating, which is also the important range in terms of the perturbation of a subionospheric probe VLF wave. In our modeling we assume the transverse variation to be proportional at all altitudes to $r^3[\exp(-0.043r)](1+\cos\psi)^{0.187}$ for $r < 70$ km and $r^{1.4}$ [exp $(-0.02r)$] $(1+\cos\psi)^{0.187}$ for $r > 70$ km (Figure 5b) where r is the radial distance and ψ is the azimuth angle measured from geomagnetic north.

4. Effect on the VLF Probe Wave

A newly developed [*Poulsen et al.*, 1992] 3-D model of subionospheric VLF propagation is used to calculate the amplitude and phase of the 24.0 kHz NAA signal along its Great Circle Path (GCP) of propagation from Cutler, Maine, to Palmer, Antarctica, both in the absence and presence of a localized ionospheric disturbance. The amplitude and phase of the vertical component of the electric field under typical ambient conditions (Profile II), assumed to be the same over all of the NAA-Palmer path, are shown in Figure 6. The signal at Palmer consists of essentially three waveguide modes, QTE_1, QTE_2 and QTM_1, with all other modes being smaller

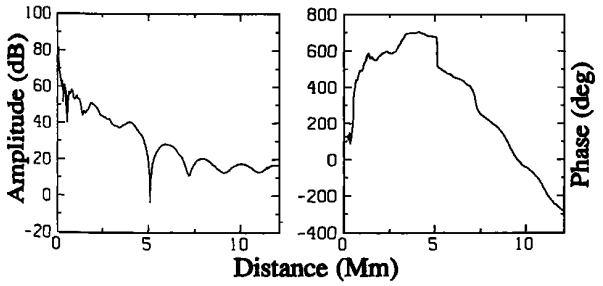

Fig. 6. The amplitude (left) and phase (right) of the 24.0 kHz NAA signal along the GCP from the source to Palmer, Antarctica. For 1 MW total radiated power from the NAA transmitter, 0 dB corresponds to 31.6 μVm^{-1}. The result shown was computed for Profile II (Figure 4a) as the ambient ionospheric electron density.

TABLE 2. Model Results

Ambient Density	Disturbance Shape	Disturbance Center	ΔA (dB)	$\Delta\phi$ (deg)
Profile II	Figure 5b	at NAU	+0.019	-0.20
Profile III	Figure 5b	at NAU	-0.003	0.00
Profile I	Figure 5b	at NAU	+0.076	-0.56
Profile II	Gaussian	at NAU	+0.009	-0.08
Profile II	Toroidal	at NAU	+0.023	-0.25
Profile II	Figure 5b	on GCP	+0.010	-0.10
Profile II	Gaussian	on GCP	+0.005	-0.03
Profile II	Toroidal	on GCP	+0.013	-0.12

than QTE_1 by >20 dB. (Here QTE or QTM designations refer to quasi-transverse electric or magnetic waveguide modes [*Poulsen et al.*, 1992].) QTE_1 has a low attenuation rate (2.1 dB/Mm over sea and 1.9 dB/Mm over land) and is generated via mode coupling along the propagation path, at the sea-land interfaces (in this case at ~2.91 Mm from NAA where the GCP crosses into the South American continent). The QTE_2 and QTM_1 mode vectors are lower in magnitude compared to QTE_1 by 14 and 16 dB respectively.

The ambient intensities of the NAA signal at Palmer are computed to be ~10, 200, and 700 μV/m for Profiles I, II, and III. In comparison with the observed range of 25-250 μV/m (Figure 3), Profile II appears to be closest to typical conditions with Profiles I and III being at the two extremes. Detectable cross modulation was observed for ambient NAA intensities of 63-175 μV/m (Figure 3, Table 1), or under conditions of moderate (Profile II) to low (Profile I) D region densities.

Amplitude (ΔA) and phase ($\Delta\phi$) changes computed for Profiles I, II, and III and the corresponding $T_n(h)$ (Figure 4b), and an ambient collision frequency profile as used in *Inan* [1990] are shown in Table 2. The disturbance was taken to be centered either at the NAU transmitter (18.42°N, 67.15°W) at a distance of ~57 km westward of the NAA-Palmer path or at the point on the GCP closest to NAU (for comparison). The transverse shape of the disturbance was taken to be that in Figure 5b, or Gaussian (i.e., proportional to exp $(-(0.005r)^2)$, or toroidal (i.e., proportional to $r^3\exp(-0.043r)$ for $r < 70$ km and to $r^{1.4}\exp(-0.02r)$ for $r > 70$ km), as indicated.

For Profile II, the 'scattered' signal at the receiver consisted primarily of QTM_1 and QTE_1 modes (QTE_1 is not generated at the disturbance but originates via mode conversion along the GCP to Palmer). In the different cases, the QTE_1 component of the 'scattered' signal was 56-73 dB lower in amplitude and lagging in phase by 168°-201° compared to the 'direct' signal. For Profile I, the dominant modes at the receiver for both the 'direct' and 'scattered' signals were QTE_1, QTM_1, and QTM_2. Much smaller ΔA and $\Delta\phi$ are expected for other signals observed at Palmer; $\Delta A = -6.4 \times 10^{-12}$ dB and $\Delta\phi = 1.7 \times 10^{-11}$ degrees for Profile II with a disturbance as shown in Figure 5*b* at NAU, for the NSS-Palmer path (at ~768 km from NAU).

5. Summary and Discussion

Results in Table 2 indicate that amplitude changes expected for the NAA-Palmer signal due to the NAU-induced disturbance range from −0.003 to +0.076 dB, in general agreement with experimental data (Table 1). The largest ΔA are expected under the most tenuous D region conditions (Profile I); such strong dependence of ΔA on ambient D region density (highly variable at night) may account for the effect's being observed in only 16 out of 144 cases. Negative ΔA are predicted for

Profile III, which may represent conditions for the events with ΔA=−0.03 and −0.04 dB (Table 1). However, the signal levels (Table 1) in these two cases were 134 and 125 μV/m respectively, closer to those predicted for Profile II.

The Gaussian disturbance leads to significantly smaller ΔA than the anisotropic (Figure 5b) or toroidal disturbances, indicating that for the parameters considered, the transverse shape is an important factor. The location of the disturbance with respect to the GCP may also be important (Table 2). The estimated phase changes of $|\Delta\phi| \leq 0.56°$ are not measurable due to the nature of the phase data, as discussed earlier.

Model results indicate that the effect of heating on the NAA-Palmer signal is enhanced under conditions of tenuous ambient D region electron density, while the ambient NAA signal levels for the observed events (Table 1, Figure 3) are more consistent with moderate conditions (Profile II). Also, events were not observed during many periods when the NAA level was similarly moderate. Aspects of the ambient nighttime ionosphere not included in our model may thus be important in the detectability of ionospheric heating by VLF waves via a VLF probe signal. The ambient electron density profile (here assumed invariant for altitudes $<\sim$95 km) may vary along the GCP and may in particular be different over NAU. Since NAU usually operated in its normal mode before and after the keying periods, the continuous heating may have slightly reduced the recombination rate, thus somewhat enhancing D region electron density [*Galejs*, 1972].

Acknowledgments. We thank R. G. Joiner and the U. S. Navy for arranging the NAU keying, our STAR Laboratory colleagues for useful discussions and Robert Drozd for his help with the data analysis. This research was supported by the Office of Naval Research under grants N00014-82-K-0489 and N00014-92-J-1579 while the VLF observations at Palmer were carried out under NSF grant DPP86-11623. J. V. Rodriguez was supported during this work by the NASA Graduate Student Researchers Program.

References

Dowden, R. L., and C. D. D. Adams, VLF versus MF heating of the lower ionosphere, *J. Geophys. Res., 96*, 14,179, 1991.

Galejs, J., Ionospheric interaction of VLF radio waves, *J. Atmos. Terr. Phys., 34*, 421, 1972.

Gurevich, A.V., *Nonlinear Phenomena in the Ionosphere*, 372 pp., Springer-Verlag, New York, 1978.

Inan, U. S., VLF heating of the lower ionosphere, *Geophys. Res. Lett., 17*, 729, 1990.

Inan, U. S., T. F. Bell, and J. V. Rodriguez, Heating and ionization of the lower ionosphere by lightning, *Geophys. Res. Lett., 18*, 705, 1991.

Maslin, N. M., Theory of energy flux and polarization changes of a radio wave with two magnetoionic components undergoing self demodulation in the ionosphere, *Proc. R. Soc. Lond. A, 341*, 361, 1974.

Poulsen, W. L., U. S. Inan, and T. F. Bell, A multiple-mode three dimensional model of VLF propagation in the Earth-ionosphere waveguide, *J. Geophys. Res.*, (in press), 1992.

Rawer, K., D. Bilitza, and S. Ramakrishnan, Goals and status of the International Reference Ionosphere, *Rev. Geophys., 16*, 177, 1978.

Taranenko, Y. N., U. S. Inan, and T. F. Bell, VLF-HF heating of the lower ionosphere and ELF wave generation, *Geophys. Res., Lett., 19*, 61, 1992.

Wait, J. R., and K. P. Spies, Characteristics of the Earth-ionosphere waveguide for VLF radio waves, *U. S. NBS Tech. Note 300*, Dec. 30, 1964.

U. S. Inan, J. V. Rodriguez, S. Lev-Tov and J. Oh, Space, Telecommunications And Radioscience Laboratory, Department of Electrical Engineering, Stanford University, Stanford, CA 94305.

(Received June 16, 1992;
revised July 30, 1992;
accepted September 17, 1992.)